American Mineralogist, Volume 76, pages 1291–1305, 1991

The role of quartz crystallization in the development and preservation of igneous texture in granitic rocks: Experimental evidence at 1 kbar

H. Elizabeth MacLellan,* Lowell T. Trembath
Department of Geology, University of New Brunswick, P.O. Box 4400, Fredericton, New Brunswick E3B 5A3, Canada

Abstract

Crystal growth experiments with haplogranodiorite compositions demonstrate that the quartz textures produced are dependent not only on degree of initial undercooling (ΔT_i) but also on duration of the crystallization experiment (t). Eight granitic compositions, H_2O-undersaturated to slightly oversaturated, were crystallized isothermally between 850 °C and 597 °C at 1 kbar for times ranging from 24 to 4320 h, producing a variety of crystal habits. Quartz crystallizes as euhedral hexagonal dipyramids, skeletal crystals, anhedral crystals, granophyric intergrowths, micropoikilitic quartz, and as a component of spherulites. Hexagonal dipyramids crystallize at small ΔT_i and are replaced by skeletal quartz at moderate to large ΔT_i. Both tend to develop modified shapes during prolonged isothermal crystallization, characterized by a reduction in the degree of faceting and, for skeletal quartz, by deep reentrants left in partially filled crystal faces. Quartz-bearing spherulites crystallize later than single crystals of quartz at moderate ΔT_i and predominate at larger ΔT_i. At moderate ΔT_i in some melt compositions, these spherulites may enclose single skeletal crystals of quartz, forming granophyric intergrowths. At large ΔT_i, granophyric intergrowths are absent but micropoikilitic quartz develops around and interstitial to the spherulites. From these results, we propose that complex granitic textures can form from sequential crystallization of two or more quartz morphologies under conditions of continuous nonequilibrium cooling and that the specific sequences vary with cooling rate as illustrated on TTM diagrams. Quartz is less susceptible than fibrous feldspars to recrystallization during the experiments and probably also during normal cooling of an igneous body. Quartz therefore provides more reliable textural information than feldspars about the cooling histories of granitic melts.

Introduction

Interpretation of the textures displayed by the common igneous rocks is a primary method used in reconstructing the cooling histories of these rocks. Experimental verification of these interpretations remains an important task. Epizonal granites and rhyolites contain abundant evidence of nonequilibrium crystallization in the form of textural heterogeneity (Buddington, 1959). Zonal variations of texture or crystallinity result from variable cooling rates across thick ash flow tuffs (Smith, 1960), epizonal granitic dykes (Stirling, 1978), and plutons (MacLellan et al., 1990). Heterogeneous textures are also common on a thin section scale, in which the morphologies and intergrowth textures of quartz and feldspar appear to have changed gradually or abruptly as crystallization proceeded (e.g., MacLellan et al., 1990; Kirkham and Sinclair, 1988; Cater, 1969). The complexity and variability of these textures renders them difficult to interpret.

A number of nonequilibrium crystallization experiments involving geologically relevant silicate melts (e.g., Lofgren, 1971, 1974; Fenn, 1977, 1986; Swanson, 1977; Swanson and Fenn, 1986; Donaldson, 1976) have shown the potential of this approach for understanding the kinetics of crystal growth and development of igneous textures. However, several factors have frequently prevented the direct reproduction and interpretation of geologically relevant textures. These factors include the relative simplicity of the compositions investigated, H_2O contents that are too high, and failure to examine the effect of time on the development of texture. For anhydrous basaltic systems at atmospheric pressure, programmed cooling experiments have been used to model directly the effect of cooling rate on development of texture, (e.g., Walker et al., 1976; Lofgren et al., 1975). For hydrous melts, it is difficult to maintain constant pressures in programmed cooling experiments (e.g., Donaldson, 1976; Lofgren and Gooley, 1977). At low, declining pressures, it is also difficult to control the amount of H_2O (Kirkpatrick, 1981) or to estimate H_2O solubility of experimental charges.

This paper describes isothermal experiments designed to simulate crystallization of granitic magmas at high lev-

* Present address: Department of Earth Sciences, Carleton University, and Ottawa-Carleton Geoscience Centre, Ottawa, Ontario K1S 5B6, Canada.

0003–004X/91/0708–1291$02.00

Table 1. Anhydrous bulk compositions used in this study

Sample	Composition
GR-1	$Ab_{34}Or_{23}An_3Q_{40}$
GR-2	$Ab_{24}Or_{33}An_3Q_{40}$
GR-3	$Ab_{34}Or_{22}An_3Q_{41}$
GR-4	$Ab_{22}Or_{34}An_3Q_{41}$
GR-7	$Ab_{34}Or_{24}An_3Q_{39}$
GR-8	$Ab_{25}Or_{33}An_3Q_{39}$
GR-9	$Ab_{35}Or_{26}An_3Q_{36}$
GR-10	$Ab_{27}Or_{34}An_3Q_{36}$

Note: Bulk compositions are expressed in weight percent.

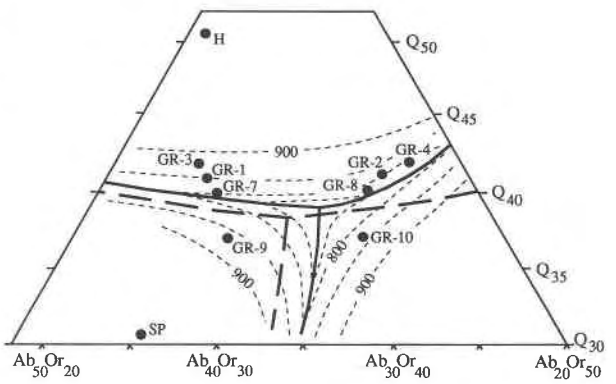

Fig. 1. Synthetic granite compositions and phase relations in a portion of the haplogranodiorite system containing 3 wt% An at 1 kbar P_T. Heavy solid lines are the liquidus phase boundaries determined from this study for a H_2O content of 3 wt%; light dashed lines are the liquidus isotherms. Heavy dashed lines are the phase boundaries in the H_2O-saturated system (James and Hamilton, 1969). GR-1–GR-4 and GR-7–GR-10 are synthetic compositions used in this study. H and SP are projections of the compositions of the Harding and Spruce Pine pegmatites, respectively, (Fenn, 1986) onto the join.

els of the Earth's crust. These experiments circumvent the difficulties associated with controlled cooling experiments under low-P, hydrous conditions by using cold-seal pressure vessels. Using H_2O-undersaturated synthetic haplogranodiorite starting compositions, the effects of initial degree of undercooling from the liquidus (ΔT_i) and experiment duration (t) have been treated as discrete variables; this was accomplished by conducting isothermal experiments of different durations at several different initial degrees of undercooling. We assume that if the bulk anhydrous compositions, H_2O contents, undercooling ranges, confining pressures, and crystallization times in these isothermal experiments are appropriate then it is possible (1) to reproduce experimentally a range of textures formed during the crystallization of similar, naturally occurring granitic melts, and (2) to predict the effect of cooling history on crystal morphologies and crystallization sequences. Comparison of these predictions with textures observed in natural granitic and rhyolitic rocks indicates that the predictions are qualitatively correct.

Isothermal experiments represent a limiting case of continuous cooling in which the cooling rate is infinitely slow. As crystallization progresses with time under isothermal conditions, the residual melt becomes progressively enriched in low-T melting components so that the actual degree of undercooling (ΔT) decreases as t increases. These conditions are probably rare in the natural environment. In natural rocks, ΔT could also increase, remain constant, or fluctuate during cooling, a range of possibilities that cannot be examined quantitatively with the method described above. Although the direction of changing ΔT conditions of the experiments over time is known, the magnitude is not. Therefore, in the discussions that follow we will use the initial undercooling (ΔT_i) in interpreting the results.

At a pressure of 1 kbar, vapor saturation of felsic magmas occurs at approximately 4 wt% H_2O (Burnham and Jahns, 1962; determined for Harding pegmatite). Granitic magmas containing more H_2O than this could not rise to a depth of less than 3.5 km (P_T = 1 kbar) in the crust without undergoing substantial crystallization during ascent (Harris et al., 1970). The corollary of this observation is that shallow intrusions emplaced at their liquidus temperature (i.e., crystal-free) must be H_2O undersaturated at the time of emplacement. In these intrusions, vapor saturation can occur at any time after the onset of crystallization, depending on the initial H_2O content and crystallization conditions. Considerations of this kind are especially important in crystallization studies because the H_2O content of the melt has a major impact on the phase relations and kinetics of crystallization of granitic magmas (Whitney, 1975; Fenn, 1977; Swanson, 1977). Therefore, H_2O contents in these experiments were generally maintained at or below 4 wt%.

The compositions prepared for the experiments were close to the minimum melt composition in the five-component haplogranodiorite system: albite (Ab)–orthoclase (Or)–anorthite (An)–quartz (Q)–H_2O (Table 1). More complex compositions were avoided because of uncertainties concerning the effects of additional components (e.g., Mg, Fe) on phase relations and reaction rates (Naney and Swanson, 1980). In contrast, the phase relations in the H_2O-saturated haplogranodiorite system are fairly well understood (James and Hamilton, 1969), and the H_2O-undersaturated phase relations can be inferred from Steiner et al. (1975) and Whitney (1975). The eight bulk anhydrous compositions contain 3 wt% An, a good approximation of the anorthite content of many naturally occurring, chemically evolved high-level granites (e.g., Barker, 1981). The compositions cluster around the piercing point of the system (Fig. 1). The effects of H_2O undersaturation are to drive the position of the piercing point and the plagioclase-alkali feldspar boundary toward the Q-Or tie line (Fig. 1) and to increase the temperatures of liquidus and subliquidus phase boundaries (Fig. 2). For GR-10, we also infer a change in the equilibrium crystallization sequence as H_2O content decreases (Fig. 2c).

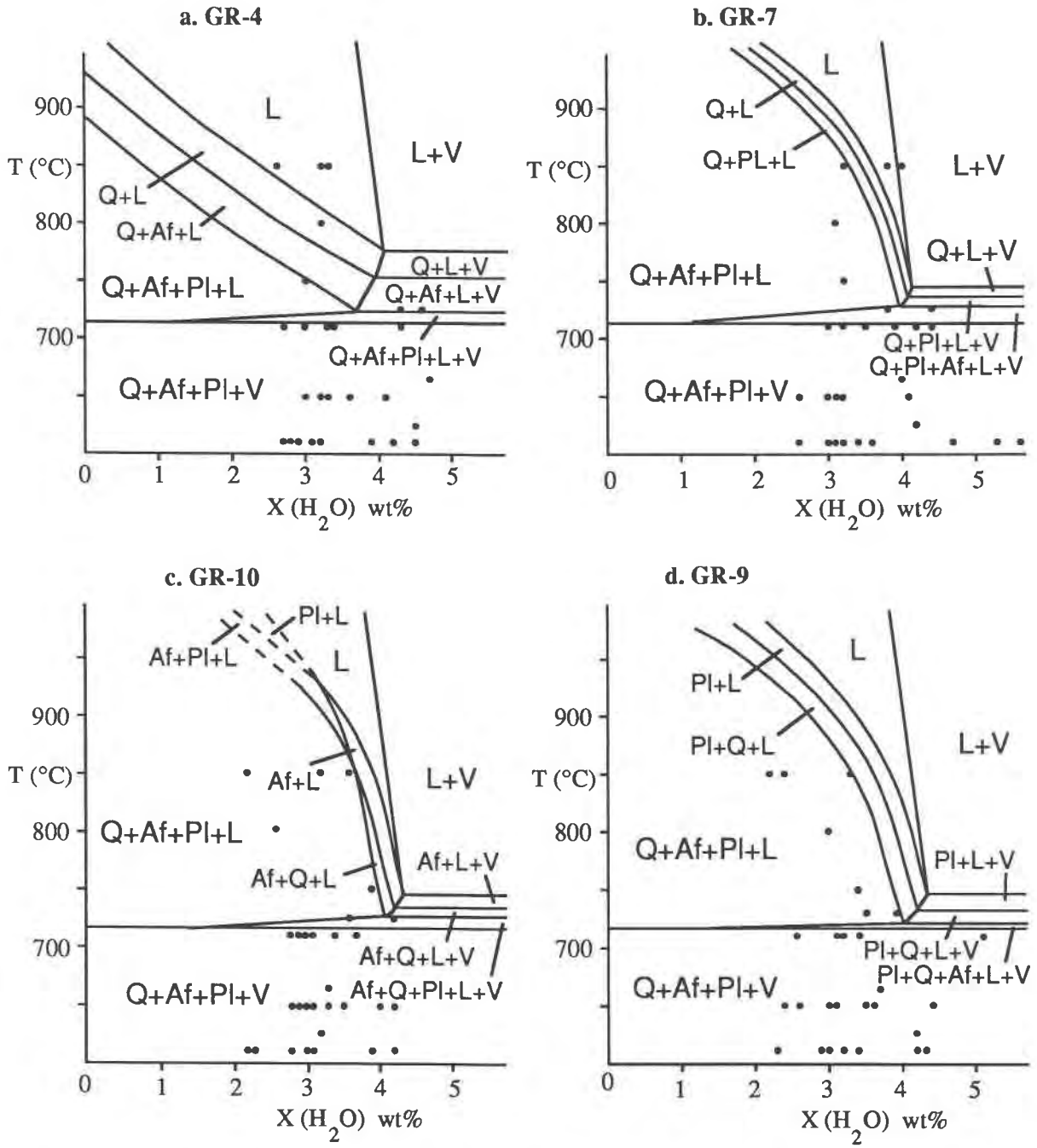

Fig. 2. Phase assemblage diagrams for selected compositions showing the effect of $X(H_2O)$ on the temperatures of the phase boundaries, inferred from James and Hamilton (1969), Whitney (1975), Steiner et al. (1975), Burnham and Jahns (1962), and this study. Solid circles = data from this study; L = liquid; V = vapor; Af = alkali feldspar; Pl = plagioclase; Q = quartz.

Experiments

Starting materials were prepared in the form of coprecipitated gels, using a method modified after Hamilton and Henderson (1968). The gels were finely ground (particle sizes <5 μm on average) with a mortar and pestle and were optically and X-ray amorphous. They were stored in an oven at 110 °C to prevent hydration. To prepare samples, weighed amounts of distilled deionized H_2O and gel were sealed in 3 mm O.D. Au capsules. The sealed samples were heated at 110 °C and 1 atm for 1 h to distribute the H_2O homogeneously and to check for leaks.

Table 2. Textural nomenclature for quartz

Quartz texture	Definition	Source
Hexagonal dipyramidal	Euhedral habit of β-quartz characterized by rhombohedral terminations $\parallel c$ with equal development of rhombohedral faces r and z (i.e., hexagonal) and by the absence or near absence of prism faces.	Frondel (1962)
Skeletal	Cellular crystal with hexagonal symmetry in which the shape has been modified by blunt protuberances developed on crystal edges and corners. Prism faces are frequently developed and crystals are commonly elongated $\parallel c$. Equivalent to the "hopper" dendrites of Fenn (1986) and to the relatively small ΔT "dendritic" morphology of Swanson and Fenn (1986).	This study
Micrographic intergrowths	Microscopic quartz-feldspar intergrowth characterized by a feldspar crystal hosting regular or cuneiform quartz rods that are in optical continuity.	Kirkham and Sinclair (1988)
Granophyric intergrowths	Microscopic quartz-feldspar intergrowth characterized by a feldspar crystal(s) hosting irregular, vermicular, or radiating quartz. The feldspar host of this study is spherulitic and the quartz is fibrous.	Kirkham and Sinclair (1988)
Micropoikilitic	"... Single crystals of quartz that enclose feldspar material, either microlites, spherulites, or fine crystals." In this study the quartz crystals poikilitically enclose or are interstitial to feldspar spherulites. Equivalent to "snowflake" texture of Anderson (1968).	Lofgren (1971)
Spherulite	"... A radiating array of crystalline fibers, all having the same fiber axis and possessing, therefore, the unusual property of branching in such a way that the crystallographic orientation of a branch departs slightly but appreciably from that of its parent fiber ... primary nuclei initiate the formation of polycrystalline aggregates which are more or less radially symmetric."	Keith and Padden (1963)
Axiolitic	Formal modifying adjective of spherulite indicating spherulitic fibers that radiate from a line and not a point.	Lofgren (1974)

The experiments were carried out in cold-seal pressure vessels of the type used by Tuttle and Bowen (1958). Pressure was generated using a hand-operated hydraulic pump rated at 40000 ψ. During heating and quenching, pressure fluctuations of ± 300 bars were unavoidable. Furnace temperatures were measured using external chromel-alumel thermocouples connected to a Consolidated Control Corp. multichannel digital recorder. The thermocouples were periodically calibrated against the melting point of NaCl and were checked against the boiling point of H_2O before each experiment. The external thermocouples did not actually measure the temperature of the samples. The temperature differences between the thermocouple positions and the sample positions were estimated to be 8–9 °C by placing an unsealed pressure vessel in each furnace with one thermocouple in the thermocouple well and another in the sample position. The reported temperatures are corrected for the systematic error in the thermocouple readings. The overall accuracy of the temperature measurements is estimated to be ± 2 °C.

Experiments were carried out in two steps. During the melt-forming step, samples were sealed in a pressure vessel at 1 kbar and melted in a furnace preheated to 850 °C. This temperature and pressure were maintained for 3 h to allow the gel to melt as completely as possible; the quenched glasses were optically homogeneous. The short melt-forming step also kept crystallization (in several of the compositions the liquidus temperatures exceed 850 °C) to a minimum. Most compositions contained anisotropic crystals that were too small to identify (<1 μm). Only GR-3, GR-9, and GR-10 contained crystal abundances great enough to be detected by powder X-ray diffraction (see Appendix Table 1). After the melt-forming step the pressure vessel was cooled under pressure with compressed air to the required crystallization temperature within 1–3 min and placed in a second furnace preheated to the desired temperature. The duration of this crystallization step varied from 24 to 4320 h, after which the pressure vessel was quenched under pressure, using compressed air to 300 °C within 3 min and to 100 °C within 10 min.

Powder X-ray diffraction scans (Cu$K\alpha$ radiation) and optical examination of grain mounts of the experimental products were used to make a preliminary identification of the crystalline phases present. Grain mounts, rather than thin sections, were used for detailed petrographic observations because the crystallized material of the samples was often friable and the amount of sample was small, making the preparation of thin sections difficult.

Results

The crystalline products of these experiments include quartz, alkali feldspar, and plagioclase. Each mineral occurs in several different habits, and more than one habit often appears in the product of a single experiment. The resulting textures of each sample are heterogeneous, but the scale of the heterogeneity is small so that all three mineral phases and most of the range of crystal morphologies and intergrowth textures are observable within a single grain of a grain mount. There is no large-scale variation in crystal size or distribution that is attributable to inhomogeneity on the scale of a charge.

Also, finely fibrous monomineralic feldspars recrystallized within the time frame of the experiments in this study, whereas quartz did not. For example, melt composition GR-10 crystallized parallel fibrous bundles of feldspar at 650 °C in 72–336 h experiments, but all longer experiments contained granular feldspars produced by recrystallization of the fibrous bundles. Most of the long duration subsolidus experiments with these melt compositions contained similar evidence of feldspar recrystallization. The feldspar morphologies and textures are described fully in MacLellan (1984).

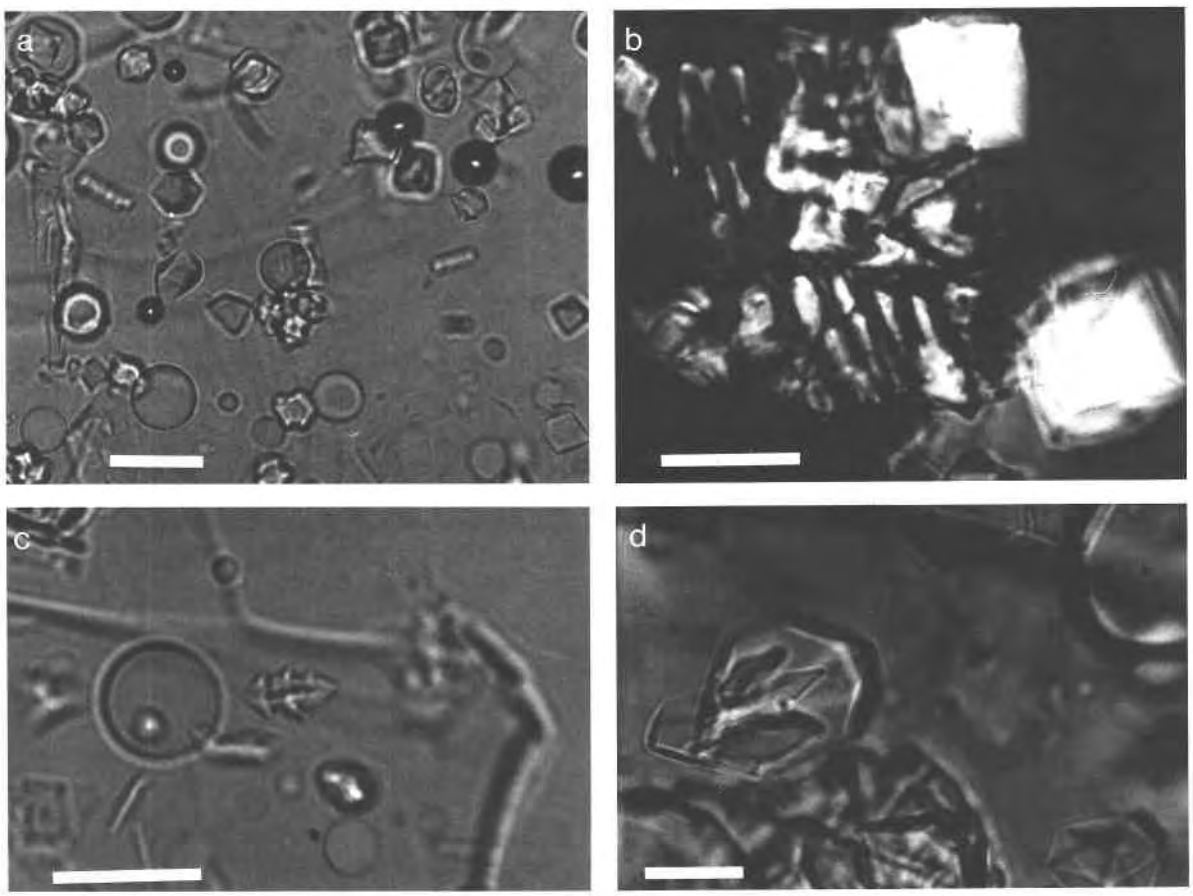

Fig. 3. Photomicrographs of quartz crystals. (**a**) Hexagonal dipyramids in a glassy matrix. GR-4: 3.0 wt% H_2O, $T = 750$ °C, $\Delta T_i = 100$ °C, $t = 842$ h. (**b**) Two dipyramidal quartz crystals with slight rounding of crystal faces and skeletal protuberances on crystal edges, and a micrographic quartz-feldspar intergrowth. GR-4: 4.6 wt% H_2O, $T = 725$ °C, $\Delta T_i = 125$ °C, $t = 2157$ h. (**c**) Skeletal quartz crystal with hexagonal pyramid terminations and elongated prism faces parallel to the **c** axis that are modified by protuberances on crystal edges and corners and embayments on crystal faces. GR-2: 3.2 wt% H_2O, $T = 710$ °C, $\Delta T_i = 150$ °C, $t = 73$ h. (**d**) Skeletal, prismatic crystal that has been partially infilled, leaving deep embayments on prism faces, from the same experiment as **b**. Scale bar = 0.02 mm.

Quartz morphologies

Quartz exhibits six distinct crystal morphologies and intergrowths, including equant hexagonal dipyramids, skeletal morphology, anhedral morphology, micrographic quartz-feldspar intergrowths, granophyric quartz-feldspar intergrowths, and micropoikilitic quartz (defined in Table 2). These crystal morphologies and intergrowth textures are illustrated in Figures 3 and 4.

The role of ΔT_i and melt composition

The results of these experiments indicate that ΔT_i has a major influence on crystal morphology but that melt composition is also an important factor. These results are illustrated in Figure 5, which shows the temperature ranges of the major quartz morphologies in all the melt compositions. On these diagrams, two solid lines join the liquidus temperatures in Or-rich and Ab-rich melts. The value of ΔT_i is the difference between the liquidus temperature and crystallization temperature.

Hexagonal dipyramidal quartz. The hexagonal dipyramid (Fig. 3a) is the high-temperature (small ΔT_i) quartz morphology in these experiments. Its lower temperature limit is a function of ΔT_i (Fig. 5a); it appears on the liquidus or quartz-feldspar boundary and disappears at ΔT_i values in the range 200–250 °C.

Skeletal quartz. At larger ΔT_i, quartz crystals develop skeletal morphologies, but the dipyramidal form is still recognizable (Table 2, Fig. 3c). The temperature range over which this morphology crystallizes in melts of different composition (Fig. 5b) is not related in a simple way to ΔT_i. Skeletal morphologies occur at small ΔT_i (<50 °C) in compositions with feldspar on the liquidus (GR-9, GR-10) and at greater ΔT_i values (50–125 °C) in the remaining compositions, which all have quartz on the liq-

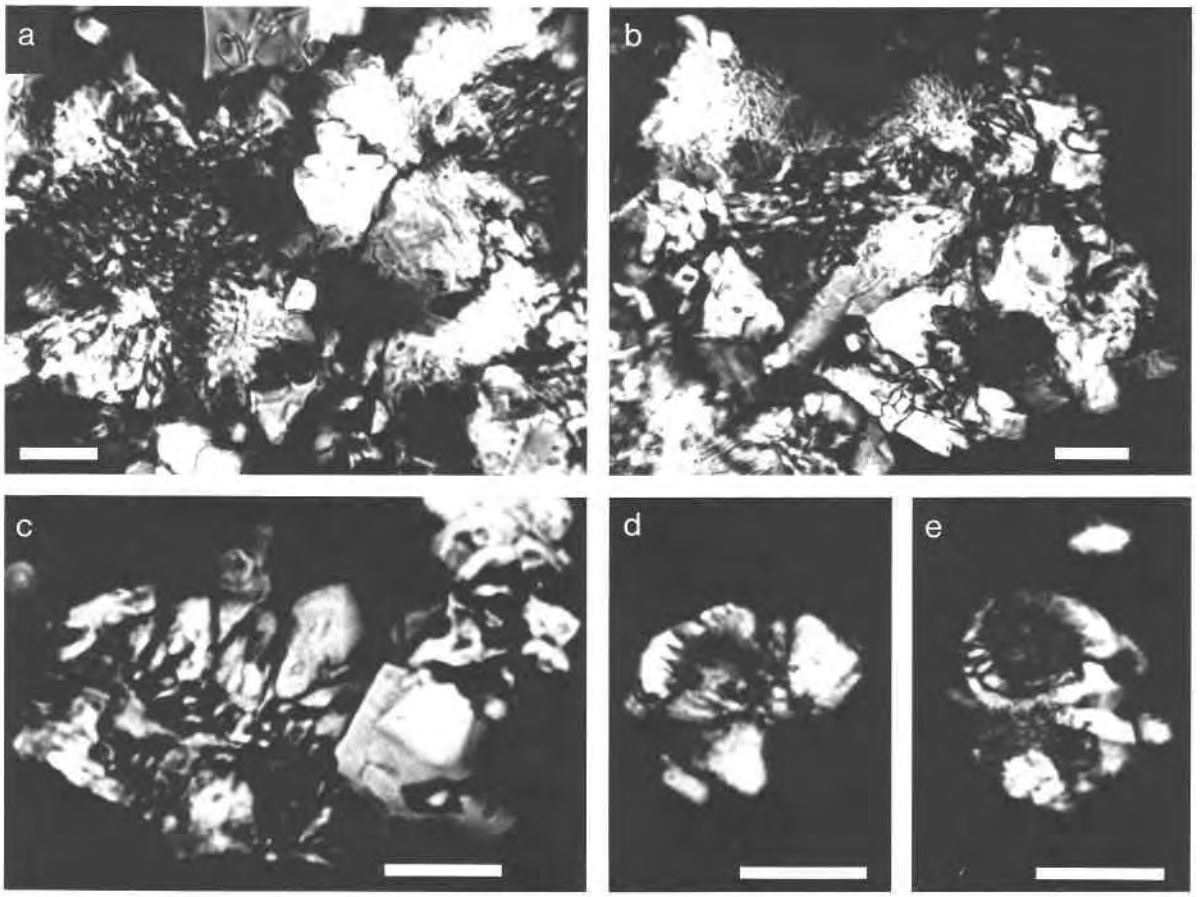

Fig. 4. Photomicrographs of granophyric intergrowths and micropoikilitic quartz. (**a**) Two large spherulites in partial extinction reveal granophyric quartz intergrown with the feldspar fibers. In the spherulite on the left, optically continuous quartz rods are seen over a large portion of the spherulite in the fuzzy extinction cross. Granophyric quartz is also formed throughout the spherulite on the right but is only distinguishable in the sector at 2 o'clock, which is at extinction. GR-8: 3.4 wt% H_2O, T = 725 °C, ΔT_i = 130 °C, t = 2157 h. (**b**) Complex intergrowth of spherulites containing granophyric quartz, from the same experiment as **a**. (**c**) Optically continuous quartz crystals growing outward from a fragment of a granophyric intergrowth (below) into glass (above); quartz crystal (slightly out of focus) indicated by the arrow has an euhedral termination. From the same experiment as **a**. (**d**) Fragment of a spherulite overgrown by micropoikilitic quartz showing detail of the spherulite-quartz interface. GR-2: 2.7 wt% H_2O, T = 650 °C, ΔT_i = 210 °C, t = 2206 h. (**e**) Optically continuous "rind" of micropoikilitic quartz encircles a spherulite (at extinction). GR-2: 2.7 wt% H_2O, T = 650 °C, ΔT_i = 210 °C, t = 2206 h. Scale bar = 0.02 mm.

uidus. In the compositions that are Or rich (GR-4, GR-2, GR-8), the ΔT_i value increases systematically as Q content of the melt increases.

Anhedral quartz. At ΔT_i > 100–150 °C, euhedral quartz crystals are rarely recognized in those experiments in which crystallization has gone to completion (Fig. 5c). Skeletal and dipyramidal crystals that were formed early generally develop prism faces or become rounded in longer experiments (Fig. 3b). Partial in-filling of crystal faces of skeletal quartz may leave deep reentrants on the faces (Fig. 3d). In several experiments, the reduction or elimination of faceting appears to have taken place before impingement on other crystals. For example, experiments at temperatures of 850 to 750 °C and durations ≥168 h using GR-3 (experiments 124-3, 127-3, and 125-3; see Appendix Table 1) and GR-9 (experiments 124-7, 127-7, and 125-7; see Appendix Table 1) formed anhedral quartz in charges that were only 40–60% crystallized. In many cases, the anhedral grains were completely surrounded by glass.

In Or-rich compositions (GR-4, GR-2, GR-8, GR-10; Fig. 5c), anhedral quartz crystallizes at greater ΔT_i than in Ab-rich compositions (GR-3, GR-1, GR-7, GR-9). In the latter, anhedral quartz may become stable at smaller ΔT_i values than skeletal quartz (compare Figs. 5b and 5c). Therefore, with increasing ΔT_i, Or-rich compositions exhibit the sequence hexagonal dipyramids → skeletal quartz → anhedral quartz, whereas Ab-rich compositions exhibit

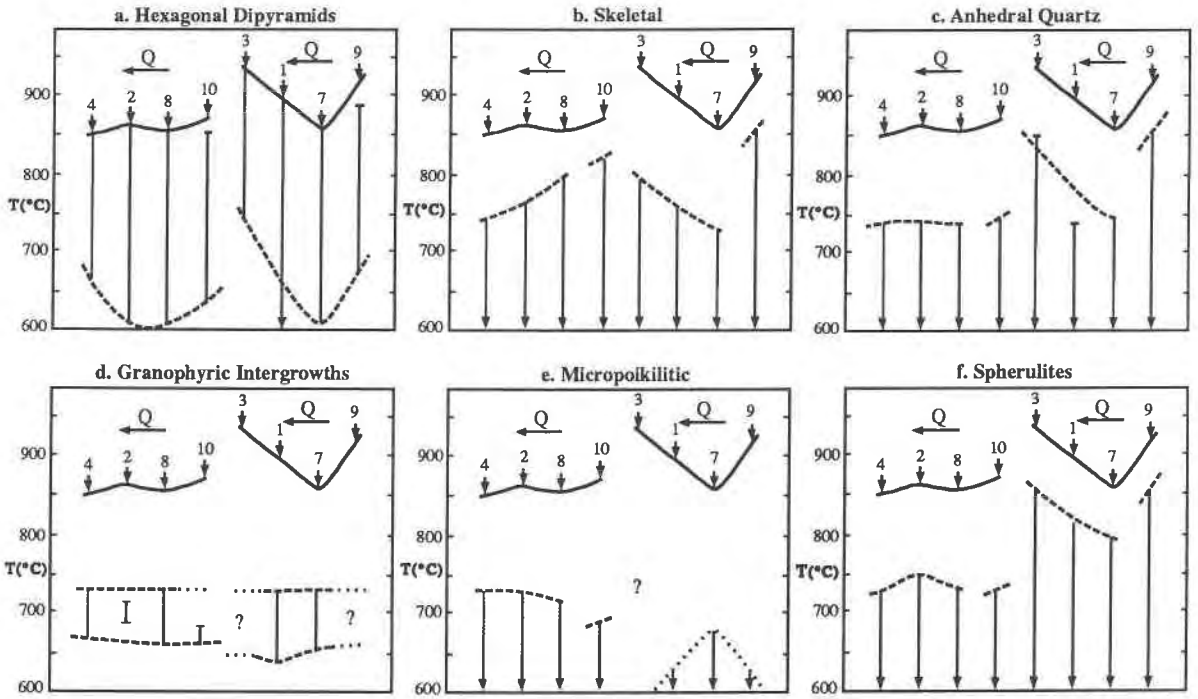

Fig. 5. Comparison of temperature ranges of quartz morphologies and spherulites crystallized from eight synthetic granites. Or-rich compositions on the left (see Fig. 1); Ab-rich compositions on the right; Q content increases from right to left in each group. Solid curves show the trend of liquidus temperature between compositions; these curves are not cross sections through the liquidus surface because compositions (marked by an arrow and number: 4 = GR-4, etc.) are plotted at equal intervals, whereas the relative changes between each composition are not all equal. GR-7 and GR-8 lie on the quartz-feldspar phase boundary (Fig. 1) and therefore in a thermal valley in these diagrams. The vertical bars indicate the temperature range over which a morphology crystallizes, with an error of ±25 °C on the upper and lower temperature limits. The dashed lines mark the trends of the upper and lower temperature limits for each morphology.

the sequence hexagonal dipyramids → anhedral quartz → skeletal quartz.

Micrographic quartz-feldspar intergrowths. Micrographic quartz as defined in Table 2 occurs in only one experiment (104-4; see Appendix Table 1 and Fig. 3b); it crystallized at 725 °C using melt composition GR-4 with 4.6 wt% H_2O. The conditions under which it can form, therefore, appear to be quite restricted. The initial conditions of this experiment were such that the ΔT_i of the melt was approximately 70 °C with respect to quartz and 25 °C with respect to the faceted alkali feldspar host (see Fig. 2a); plagioclase did not crystallize. Fenn (1986) has experimentally produced micrographic textures using Spruce Pine and Harding pegmatite compositions (see Fig. 1) only in composition-temperature regions with ΔT_i values slightly greater than that of the quartz-feldspar cotectic, conditions similar to those described above.

Granophyric quartz-feldspar intergrowths. The most common quartz-feldspar intergrowth in the experiments is granophyric (Table 2, Figs. 4a and 4b). The feldspar host to the granophyric intergrowths is spherulitic and probably contains both alkali feldspar and plagioclase. The optically continuous quartz fibers tend to coarsen outward from the center of the spherulite. The scale of the intergrowth is very fine (<1 μm fiber width) and is often only recognizable by the simultaneous extinction of the quartz rods or fibers within a sector of the spherulite (see Fig. 4a). The largest ΔT_i of the feldspar that is host to the granophyric intergrowths of this study is greater than that of the feldspar host to the micrographic intergrowths described above and by Fenn (1986). For example, melt compositions GR-4 and GR-7 crystallized granophyric intergrowths at 665 °C (experiments 102-4, 102-5; see Appendix Table 1) with the ΔT_i of the melt of approximately 110 °C with respect to quartz and 85 °C with respect to the quartz-feldspar cotectic.

The temperature-composition pattern of granophyric intergrowths differs from those of other morphologies. For compositions in which this form is common (GR-4, GR-8, GR-1, GR-7, Fig. 5d, Appendix Table 1), granophyric quartz occurs within a nearly constant temperature range (approximately 730–650 °C). In GR-2 and GR-10, granophyric intergrowths appear sporadically. Two of the compositions having quartz and plagioclase on the liquidus (GR-3 and GR-9, respectively), failed to develop any granophyric intergrowths. These two melts are the

most highly undercooled (ΔT_i with respect to the liquidus >170 °C; ΔT_i with respect to the cotectic >130 °C) and have the highest crystallization rates (see Appendix Table 1) in the temperature range over which granophyric textures formed.

Micropoikilitic quartz. Micropoikilitic quartz as defined in Table 2 crystallizes in relatively long experiments at ΔT_i > 120–170 °C (Fig. 5e). At moderate ΔT_i, micropoikilitic quartz is often associated with granophyric quartz-feldspar intergrowths, forming optically continuous outgrowths of the granophyric quartz past the edge of the spherulitic host into the glass (Fig. 4c); pyramidal terminations may be developed on these outgrowths.

Although the ΔT ranges of granophyric and micropoikilitic quartz overlap in most melt compositions, micropoikilitic quartz always persists to lower temperatures than granophyric intergrowths. At large ΔT_i in the absence of granophyric quartz, micropoikilitic quartz usually occurs as thin, optically continuous, interstitial rinds coating groups of spherulites or feldspar crystals (Figs. 4d, 4e), and pyramidal terminations are much less common than at smaller ΔT_i values. The micropoikilitic quartz textures produced during this study are similar to those described by Lofgren (1971) in devitrification products of highly undercooled natural rhyolite glasses (T = 100–700 °C, P_T = 0.001–4.0 kbar). These glasses were devitrified in the presence of higher H_2O contents (9–20 wt%) and alkalies than were used in this study. The resultant micropoikilitic quartz textures were coarser and more abundant than those observed here.

The apparent effect of bulk composition on the range of crystallization temperatures of micropoikilitic quartz (Fig. 5e) is difficult to interpret. In Or-rich compositions, micropoikilitic quartz crystallizes at moderate ΔT_i but appears at progressively smaller ΔT_i values as the Q content of the melt increases. However, in Ab-rich compositions, the higher the liquidus temperature the greater the degree of undercooling required for its formation. It is possible that this difference is an artifact of the experimental method, in which the melt-forming step took place at a temperature significantly below the liquidus for compositions with relatively high liquidus temperatures. Compositions with the highest liquidus temperatures (GR-3 and GR-9) form micropoikilitic quartz at the greatest ΔT_i values and do not form granophyric intergrowths at all. For those compositions in which granophyric intergrowths form, micropoikilitic quartz occurs later in time or at relatively greater ΔT_i.

Spherulites. Spherulites and axiolitic spherulites comprised of two or more minerals (alkali feldspar, plagioclase, quartz) are formed at ΔT_i >50–225 °C (Fig. 5f). These morphologies are finely fibrous (terminology of Keith and Padden, 1963) and become finer with increasing ΔT_i. Spherulites formed at relatively small ΔT_i may be host to granophyric quartz. Only nongranophyric spherulites occur at large ΔT_i; quartz may still be present in these spherulites although its presence cannot be confirmed optically. Spherulites first appear at smaller values of ΔT_i in Ab-rich melts than in Or-rich melts (Fig. 5f).

The role of t in isothermal experiments

The crystal morphologies and intergrowth textures produced by isothermal experiments of different duration can vary dramatically. For all melt compositions, experiments of short duration contain only one or two quartz morphologies. With increasing duration, the number of quartz morphologies and complexity of the textures increase. Time-related crystallization sequences are different at different ΔT_i. The time-temperature relationships of the crystal morphologies and intergrowth textures are somewhat different for each melt composition examined. These observations are illustrated with time-temperature morphology (TTM) diagrams in Figure 6. Compositions GR-4, GR-7, and GR-10 were chosen to illustrate the utility of this approach because they were relatively slow crystallizing, thus providing the greatest amount of information about isothermal crystallization sequences. Curves on the diagrams mark the occurrence in time-temperature space of the different morphologies and intergrowths.

Two different types of processes affect the isothermal crystallization sequences. One involves a change in crystal habit during the growth process. For example, in GR-10 at ΔT_i = 40 °C (Fig. 6c), hexagonal dipyramids formed in short experiments, whereas both skeletal and dipyramidal habits formed in longer experiments (see Appendix Table 1); the skeletal crystals formed during continued crystallization of dipyramids that formed early. In GR-4 at ΔT_i = 140 °C (Fig. 6a), dipyramidal and skeletal quartz cocrystallize in short experiments; in longer experiments (t > 700 h), the quartz is anhedral; this shape has evolved during continued crystallization of the crystals that formed initially. The curves for skeletal and anhedral quartz in Figure 6 mark this evolution of one morphology into another (i.e., hexagonal dipyramids → skeletal quartz; skeletal quartz → anhedral quartz). This type of process produces textural modification over time without increasing textural complexity.

The second type of process, which is synchronous with the first, involves the sequential crystallization of different crystal morphologies or mineral intergrowths. For example, in GR-4 at ΔT_i = 140 °C (Fig. 6a), the isothermal crystallization sequence is dipyramidal + skeletal quartz followed by skeletal quartz + granophyric intergrowths followed by anhedral quartz + granophyric intergrowths + micropoikilitic quartz. The curves for hexagonal dipyramids, granophyric intergrowths, and micropoikilitic quartz indicate their incubation periods as a function of ΔT_i (and T). This process of sequential crystallization produces an increase in textural complexity over time as crystallization proceeds.

Discussion

Crystallization conditions of quartz morphologies

The hexagonal dipyramidal quartz morphology is the euhedral habit of β-quartz that forms at small ΔT_i values. Faceted morphologies like this are considered to form by one of several possible interface-controlled growth mech-

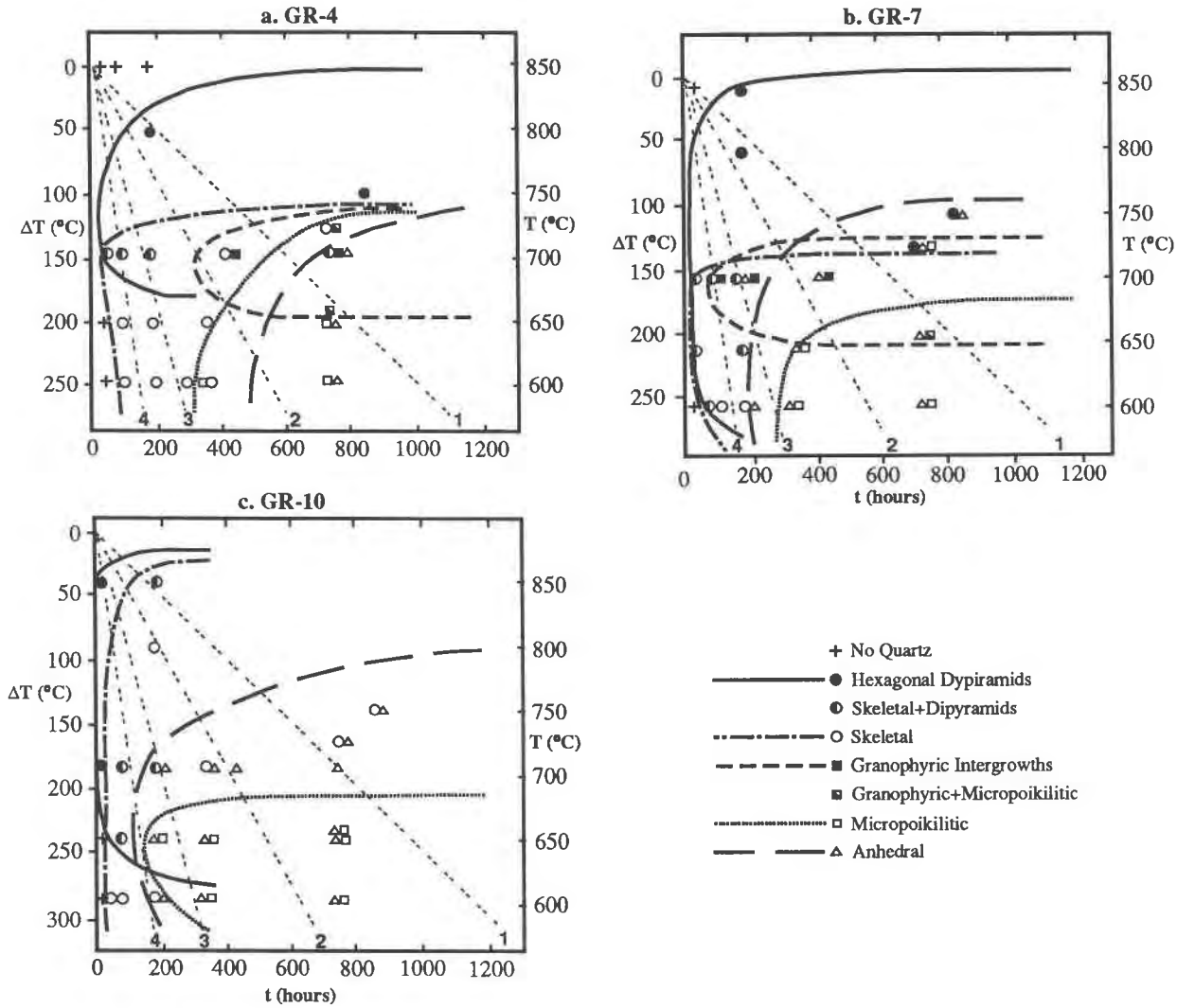

Fig. 6. Time-temperature-morphology (TTM) curves of quartz morphologies crystallizing from (a) composition GR-4, (b) composition GR-7, and (c) composition GR-10 at 1 kbar P_T. Curves mark the occurrence of quartz morphologies in time-temperature space. Symbols indicate experimental results. The dashed lines numbered 1–4 represent four different constant cooling rates from the liquidus.

anisms (e.g., Kirkpatrick, 1981). The presence of the skeletal morphology indicates that ΔT_i is sufficiently large to produce conditions of diffusion-controlled growth. In an undercooled melt that has developed compositional gradients at the crystal-melt interface, the attachment kinetics are facilitated at crystal edges and corners relative to crystal faces (Kirkpatrick, 1981). This is because the larger melt volume to surface ratio at the corners and edges allows more efficient diffusion of rejected components away from these locations. As a result, the interface melt composition is closer to the bulk melt composition, the local undercooling is greater, and the growth rate is faster. Increasing Q content of the melt delays the onset of skeletal crystallization until more undercooling has occurred by reducing the rate at which the compositional gradients are developed.

Fenn (1986) has demonstrated that micrographic textures are dependent on local kinetics at the crystallizing growth front of the feldspar host. They form at temperatures close to the quartz-feldspar cotectic where ΔT_i relative to the feldspar host is small enough to stabilize a planar-growth interface. The mechanism proposed by Fenn to explain the development of graphic texture involves the development of a boundary layer enriched in SiO_2 and H_2O at the growing feldspar interface. A condition of constitutional supercooling is created (e.g., Lofgren, 1974; Kirkpatrick, 1975) with the ΔT of the melt increasing with distance from the crystal-melt interface. As a result, random protuberances formed on the growing feldspar surface grow spontaneously, causing a breakdown of the interface from planar to cellular and concentrating SiO_2 between the cell boundaries. The SiO_2 con-

tent of the intercellular liquid achieves a level of supersaturation that allows one or more skeletal quartz crystals to nucleate and grow along with the feldspar.

Granophyric intergrowths appear to be textures that are transitional between relatively small ΔT end-members (graphic intergrowths) and large ΔT end-members (quartz-bearing spherulites). The data presented in this study suggest that they crystallize by a mechanism similar to that proposed by Fenn for graphic intergrowths but under conditions of relatively greater ΔT_i with respect to the feldspar host and the quartz-feldspar cotectic. The greater ΔT values cause the feldspar host of the granophyric intergrowth to be spherulitic. Granophyric intergrowths develop over a temperature interval of approximately 80 °C with an upper temperature limit defined by the quartz feldspar cotectic if (1) the melt is not highly undercooled in this temperature interval (e.g., ΔT_i with respect to the liquidus <150 °C; ΔT_i with respect to the cotectic is approximately 25–115 °C in this study) and (2) the melt composition is close to the minimum melt composition. The second criterion is essential to the attainment of the first because it results in a reduction in liquidus temperatures relative to solidus temperatures. Relatively slow rates of nucleation may also be required, particularly in the case of quartz, and in this regard H_2O may play a role. In the relatively long experiments in which granophyric intergrowths are most likely to occur, the texture is more prevalent in those experiments with relatively high H_2O content (Appendix Table 1). Because the effect of high H_2O content in the melt is to reduce rates of nucleation and crystal growth (e.g., Fenn, 1977) and the temperature interval between the liquidus and solidus (e.g., Whitney, 1975), its presence should further enhance the effects described above.

Quartz with micropoikilitic texture is the lowest temperature nonfibrous crystal morphology and is the last to crystallize in isothermal experiments. Nevertheless, this form of quartz has been observed in experiments with substantial amounts of residual glass. The observation of feldspar-bearing spherulites, rimmed by micropoikilitic quartz and, in turn, surrounded by glass (e.g., GR-8, experiment 104-6, Fig. 4c and Appendix Table 1; GR-4, experiment 122-4, Appendix Table 1) suggests that micropoikilitic quartz forms from a SiO_2- (and H_2O-) enriched boundary layer that accumulates during growth of a spherulite in a manner similar to that of graphic and granophyric intergrowths. However, in the formation of micropoikilitic quartz, these impurities must build up ahead of the advancing growth front of the spherulite until local supersaturation occurs with respect to the quartz, which crystallizes as an interstitial or micropoikilitic crystal. This process generally requires similar ΔT values and longer t or larger ΔT values than that which produces granophyric intergrowths.

Relationship between cooling history and quartz textures

In a study of olivine nucleation, Donaldson (1979) demonstrated that nucleation is delayed in programmed cooling experiments compared with isothermal experiments. Therefore, curves of olivine incubation plotted on a time vs. temperature diagram are similar in form, but the curve constructed from continuous cooling experiments is shifted to greater ΔT than the one constructed from isothermal experiments. Although the melt compositions are different, a similar conclusion can be inferred for the experimental results reported here. Therefore, the exact position and shape of any morphology curve in Figure 6 could be expected to vary as a function of cooling rate. Even so, it may be feasible to make qualitative predictions about the effect of variable cooling rates on crystallization sequences of quartz using these diagrams. To illustrate how such predictions can be made, lines representing contrasting rates of continuous cooling have been superimposed on the TTM curves in Figure 6. Crystallization sequences predicted for a given cooling rate are somewhat different for different melt compositions.

For a slow cooling rate in composition GR-4 (line 1, Fig. 6a), quartz will develop first with a hexagonal dipyramidal habit at small ΔT, but these crystals will become skeletal or anhedral as cooling continues, and some crystals may have reentrants. Subsequently, granophyric intergrowths will form near the solidus and may be overgrown by micropoikilitic quartz like that shown in Figure 4c. At a somewhat higher cooling rate (line 2, Fig. 6a), early-formed hexagonal dipyramids will become skeletal during continued growth; granophyric intergrowths with quartz overgrowths will develop later. Crystallization may be complete before the field of anhedral quartz is reached in time-temperature space. If the cooling rate is higher still (line 3, Fig. 6), skeletal quartz will develop rapidly from hexagonal dipyramidal precursors; granophyric intergrowths will not form, but micropoikilitic quartz may still form around spherulites if crystallization continues to large undercoolings (>300 °C). For the highest cooling rate (line 4, Fig. 6a), hexagonal dipyramids will crystallize, but planar interfaces will break down during growth resulting in skeletal crystals. Micropoikilitic quartz will form at a later stage. For cooling rates even higher than that represented by line 4, hexagonal dipyramids of quartz will form and will not evolve into skeletal crystals.

Comparison of natural and synthetic quartz morphologies and intergrowth textures

The hexagonal dipyramid is a typical morphology of β-quartz in natural rocks (Frondel, 1962) and commonly occurs as phenocrysts in rhyolites. However, the skeletal quartz described above is not a typical morphology of quartz in natural granitic rocks, and the time-related experiments provide an explanation for this apparent discrepancy by demonstrating that prolonged crystallization of quartz crystals results in modifications of dipyramidal or skeletal morphologies that were formed early. At moderate to large ΔT_i, continued crystallization of early skeletal quartz can produce partial in-filling of crystal faces. In both dipyramidal and skeletal quartz, continued crystallization is also accompanied by reduction in the degree

of faceting of the crystals; edges and corners become rounded and faces become curved for reasons that are not understood. The result can be deep reentrants extending inward from rounded crystal faces. This observation suggests that naturally occurring embayed quartz phenocrysts in rhyolites and granites may also be a normal result of crystallization under conditions of moderately high cooling rate. Swanson and Fenn (1986) have suggested a similar interpretation for the formation of embayed volcanic phenocrysts lacking any apparent corona or other reaction relation or of those that are enclosed by a quartz-bearing groundmass. Thus, in the absence of corroborating evidence (see Donaldson and Henderson, 1988), the presence of rounded quartz phenocrysts with reentrants in volcanic rocks should not be interpreted to indicate that quartz has been resorbed.

Two types of micropoikilitic quartz occur in the experiments. At moderate ΔT values, micropoikilitic quartz is sometimes associated with granophyric intergrowths and overgrows them; a similar texture has been described in natural granites (e.g., Smith, 1974; White et al., 1981, Fig. 23). Micropoikilitic texture most commonly forms at large values of ΔT in experiments, and examples of natural textures like these are described by Geijer (1913), Anderson (1968), and Swanson et al. (1989) from volcanic rhyolites.

One of the major differences between the experiments and natural granites appears to be the morphology of the feldspar in the quartz-feldspar intergrowths. The spherulitic feldspar hosts of granophyric quartz that occur in the experiments are rarely reported in naturally occurring radiating granophyric intergrowths. Natural micropoikilitic quartz or snowflake texture (e.g., Anderson, 1968) commonly contains poikilitically enclosed feldspar microlites rather than the spherulites observed in these experiments. The differences may result from recrystallization of fibrous feldspars. This line of reasoning is supported by the observation that finely fibrous monomineralic feldspars recrystallized within the time frame of the laboratory experiments in this study. The feldspars must undergo substantial modifications of chemical composition and structural state if they are to remain in equilibrium during cooling of igneous rocks (e.g., Smith, 1974). This process requires the breaking of chemical bonds, which may facilitate recrystallization. On the other hand, quartz remains chemically and structurally stable under conditions of decreasing temperature expected during normal cooling of felsic igneous bodies (Tuttle and Bowen, 1958); the α-β transition is spontaneous and unquenchable. The relative chemical and structural stability of quartz should render it far less susceptible to recrystallization and textural modification than the fibrous feldspars, which appear to recrystallize under most geologically relevant conditions and are unlikely to be preserved in natural granites. Therefore, quartz morphologies should provide much more reliable information about cooling histories of granitic melts than the feldspars.

Recrystallization of spherulites in micropoikilitic quartz from natural granites could conceivably produce a texture similar to that of granophyric intergrowths, as suggested by Lofgren (1971). In this event, micropoikilitic quartz should still be distinguishable from micrographic and granophyric quartz on the basis of texture. Micropoikilitic quartz will have irregular patterns of stubby quartz blebs and shreds (Lofgren, 1971). Granophyric quartz will have elongate and vermicular or radiating patterns of growth (Sinclair et al., 1988; Fig. 6). Both of these quartz-feldspar intergrowths are readily distinguished from the micrographic intergrowths that contain elongate cuneiform quartz rods (Kirkham and Sinclair, 1988; Fig. 4d). Devitrification textures that occur in densely welded ash flow tuffs (referred to as granophyric by Smith, 1960) may in some cases be classified as micropoikilitic according to the above criteria.

Epizonal plutons and subvolcanic stocks often have complex textures with more than one generation of quartz that are similar to the predicted crystallization sequences described above for conditions of nonequilibrium cooling. Seriate granite with granular, anhedral quartz in a microgranophyric groundmass described by MacLellan et al. (1990) has a texture very similar to that predicted for slow cooling of GR-7 (line 1, Fig. 6b). Subvolcanic granite with a similar texture (White et al., 1981), in which the micrographic intergrowths of the groundmass are overgrown by quartz, are like those predicted for slow to moderate cooling rates in GR-4 (lines 1 and 2, Fig. 6a). Granodiorite containing granular quartz with reentrants and later, interstitial (micropoikilitic equivalent?) quartz (Cater, 1969) has a crystallization sequence similar to that predicted for slow to moderate cooling of GR-10 (lines 1 and 2, Fig. 6c). Porphyritic aplites in which quartz occurs as phenocrysts, as groundmass grains, and as granophyric intergrowths that occur in the groundmass or overgrow phenocrysts (Kirkham and Sinclair, 1988) are similar to textures predicted for rapid cooling of GR-7 (lines 3 and 4, Fig. 6b), assuming that the quartz phenocrysts were already present.

Conclusion

In the haplogranodiorite melts reported here, hexagonal dipyramids of quartz crystallize at small ΔT_i. At progressively larger ΔT_i, quartz crystallizes as skeletal crystals, granophyric to fibrous quartz-feldspar intergrowths, and micropoikilitic quartz. Similar observations have been made by Swanson (1977), Swanson and Fenn (1986), and Lofgren (1971).

The crystal-growth experiments have further demonstrated that quartz morphologies, textures of quartz-feldspar intergrowths, and crystallization sequences in granitic melts are dependent not only on ΔT_i but also on the duration of the crystallization experiment and melt composition. TTM diagrams for three of the granite compositions illustrate the importance of considering the role of time on the crystallization behavior of granitic rocks. In isothermal experiments, the number of quartz morphologies increases with increasing t. From this result, it is inferred that a granitic melt cooling at a constant rate may crystallize quartz having two or more morphologies at

different stages in its cooling history. Therefore, the observation of a sequential change in quartz morphology in a granitic rock need not be explained by sudden changes in pressure, temperature, or fluid content in the absence of other evidence such as a concomitant change in grain size. Instead, the observation of a particular set of morphologies may simply indicate that the melt has undergone nonequilibrium crystallization under specific conditions of continuous cooling.

These results fall short of providing a quantitative model for evaluating the cooling history of a granitic melt on the basis of its quartz textures. Nonetheless, the experimentally produced quartz morphologies and quartz-feldspar intergrowths bear a close resemblance to natural analogues and the predicted effect of increasing cooling rates on quartz morphologies provides a coherent framework for the qualitative interpretation of granitic texture and textural variations within and between granitic and rhyolitic rock types.

Acknowledgments

This work was funded by NSERC operating grant to L.T.T. Additional funding was provided by R.P. Taylor through a NSERC operating grant. Earlier versions of this manuscript were critically reviewed by R.J. Kirkpatrick, P.M. Fenn, S.E. Swanson, and A.D. Fowler, and the presentation of the results has been greatly improved thanks to their helpful comments.

References cited

Anderson, J.E. (1968) Development of snowflake texture in a welded tuff, Davis Mountain, Texas. Geological Society of America Bulletin, 80, 2075–2080.

Barker, F., Ed. (1981) Granites and rhyolites. Journal of Geophysical Research, Special Issue, 86, 10131–10633.

Buddington, A.F. (1959) Granite emplacement with special reference to North America. Bulletin of the Geological Society of America, 70, 671–747.

Burnham, C.W., and Jahns, R.H. (1962) A method for determining the solubility of water in silicate melts. American Journal of Science, 260, 721–745.

Cater, F.W. (1969) The Cloudy Pass epizonal batholith and associated subvolcanic rocks. Geological Society of America Special Paper 116, 54 p.

Donaldson, C.H. (1976) An experimental investigation of olivine morphology. Contributions to Mineralogy and Petrology, 57, 187–213.

——— (1979) An experimental investigation of the delay in nucleation of olivine in mafic magmas. Contributions to Mineralogy and Petrology, 69, 21–32.

Donaldson, C.H., and Henderson, C.M.B. (1988) A new interpretation of round embayments in quartz crystals. Mineralogical Magazine, 52, 27–33.

Fenn, P.M. (1977) The nucleation and growth of alkali feldspars from hydrous melts. Canadian Mineralogist, 15, 135–161.

——— (1986) On the origin of graphic granite. American Mineralogist, 71, 325–330.

Frondel, C. (1962) The system of mineralogy, vol. 3: Silica minerals (7th edition), 334 p. Wiley, New York.

Geijer, Per. (1913) On poikilitic intergrowths of quartz and alkali feldspar in volcanic rocks. Geologiska Foereningens i Stockholm, Foerhhandlinger, 35, 51–80.

Hamilton, D.L., and Henderson, C.M.B. (1968) The preparation of silicate compositions by a gelling method. Mineralogical Magazine, 36, 832–838.

Harris, P.G., Kennedy, W.Q., and Scarfe, C.M. (1970) Volcanism versus plutonism—the effect of chemical composition. Geological Journal Special Issue 2, 187–200.

James, R.S., and Hamilton, D.L. (1969) Phase relations in the system $NaAlSi_3O_8$-$KAlSi_3O_8$-$CaAl_2Si_2O_8$-SiO_2 at 1 kilobar water vapour pressure. Contributions to Mineralogy and Petrology, 21, 111–141.

Keith, H.D., and Padden, F.J., Jr. (1963) A phenomenological theory of spherulitic crystallization. Journal of Applied Physics, 34, 2409–2421.

Kirkham, R.V., and Sinclair, W.D. (1988) Comb quartz layers in felsic intrusions and their relationship to porphyry deposits. Canadian Institute of Mining and Metallurgy Special Volume 39, 50–71.

Kirkpatrick, R.J. (1975) Crystal growth from the melt: A review. American Mineralogist, 60, 798–814.

——— (1981) Kinetics of crystallization in igneous rocks. In Mineralogical Society of America Reviews in Mineralogy, 8, 321–398.

Lofgren, G. (1971) Experimentally produced devitrification textures in natural rhyolitic glass. Geological Society of America Bulletin, 82, 111–124.

——— (1974) An experimental study of plagioclase crystal morphology: Isothermal crystallization. American Journal of Science, 274, 243–273.

Lofgren, G.E., and Gooley, R. (1977) Simultaneous crystallization of feldspar intergrowths from the melt. American Mineralogist, 62, 217–228.

Lofgren, G.E., Donaldson, C.H., and Usselman, T.M. (1975) Geology, petrology and crystallization of Apollo 15 quartz-normative basalts. Proceedings of the Sixth Lunar Science Conference, 79–99.

MacLellan, H.E. (1984) Experimental study of dynamic crystallization in synthetic granite melts at 1 kilobar, 216 p. Unpublished M.Sc. thesis, University of New Brunswick, Fredericton, New Brunswick, Canada.

MacLellan, H.E., Taylor, R.P., and Gardiner, W.W. (1990) Geology and geochemistry of Middle Devonian Burnthill Brook granites and related tin-tungsten deposits, York and Northumberland counties, New Brunswick (Canada). Mineral Resource Report 4, 95 p. New Brunswick Department of Natural Resources and Energy, Minerals and Energy Division, New Brunswick, Canada.

Naney, M.F., and Swanson, S.E. (1980) The effect of Fe and Mg on crystallization in granitic systems. American Mineralogist, 65, 639–653.

Sinclair, W.D., Kooiman, G.J.A., and Martin, D.A. (1988) Geological setting of granites and related tin deposits in the North Zone, Mount Pleasant, New Brunswick. Geological Survey of Canada, Paper 88-1B, 201–208.

Smith, J.V. (1974) Feldspar minerals. 2: Chemical and textural properties, 690 p. Springer-Verlag, New York.

Smith, R.L. (1960) Zones and zonal variations in welded ash flows. United States Geological Survey Professional Paper 354-F, 149–159.

Steiner, J.C., Jahns, R.H., and Luth, W.C. (1975) Crystallization of alkali feldspar and quartz in the haplogranite system $NaAlSi_3O_8$-$KAlSi_3O_8$-SiO_2-H_2O at 4 kb. Bulletin of the Geological Society of America, 86, 83–98.

Stirling, J.A.R. (1978) Crystallization of a felsic dyke. Unpublished M.Sc. thesis, University of New Brunswick, Fredericton, New Brunswick, Canada.

Swanson, S.E. (1977) Relation of nucleation and crystal growth to the development of granitic textures. American Mineralogist, 62, 966–978.

Swanson, S.E., and Fenn, P. (1986) Quartz crystallization in igneous rocks. American Mineralogist, 71, 331–342.

Swanson, S.E., Naney, M.T., Westrich, H.R., and Eichelberger, J.C. (1989) Crystallization history of Obsidian Dome, Inyo Domes, California. Bulletin of Volcanology, 51, 161–176.

Tuttle, O.F., and Bowen, N.L. (1958) Origin of granite in the light of experimental studies in the system $NaAlSi_3O_8$-$KAlSi_3O_8$-SiO_2-H_2O. Geological Society of America Memoir 74, 153 p.

Walker, D., Kirkpatrick, R.J., Longhi, J., and Hays, J.F. (1976) Crystallization history of lunar picrite basalt sample 12002: Phase equilibria and cooling rate studies. Geological Society of America Bulletin, 87, 646–656.

White, W.H., Bookstrom, A.A., Kamilli, R.J., Ganster, M.W., Smith, R.P., Ranta, D.E., and Steininger, R.C. (1981) Character and origin of Climax-type molybdenum deposits. Economic Geology, 75th Anniversary Volume, 270–316.

Whitney, J.A. (1975) The effects of pressure, temperature, and X_{H_2O} on phase assemblage in four synthetic rock compositions. Journal of Geology, 83, 1–31.

Manuscript received July 14, 1989
Manuscript accepted April 16, 1991

APPENDIX TABLE 1. Experimental conditions and quartz morphologies observed in the experimental products

Run no.	T (°C)	t (h)	H_2O (wt%)	Morphology HD	SK	GR	MP	AN	Approx. % glass	Run no.	T (°C)	t (h)	H_2O (wt%)	Morphology HD	SK	GR	MP	AN	Approx. % glass
Granite GR-4										**Granite GR-8**									
89-1	850	3	3.2						100	88-4	850	3	1.5						100
87-5	850	24	2.6						100	86-4	850	24	2.3	x					100
124-4	850	170	3.3						100	124-6	850	170	3.2	X					99
127-4	800	168	3.2	X					95	127-6	800	168	2.7	X	X				95
125-4	750	842	3.0	X					90	125-6	750	842	3.1	X	X				90
101-3	725	720	4.3	X	X	X	x		60	101-5	725	720	4.1	X	X	X			60
104-4	725	2157	4.6	X	X	X	X	X	50	104-6	725	2157	3.4			X		X	30
95-4	710	24	4.3	X	X				99	90-6	710	24	4.8	X					98
90-4	710	24	3.3	X	X				95	95-6	710	24	2.8	X					98
121-4	710	73	3.4	X	X				95	98-6	710	72	3.5	X	X				98
98-4	710	72	2.7	X	X				95	128-3	710	73	3.0	X	X				90
92-4	710	168	3.3	X	X				95	121-6	710	73	2.8	X	X				90
120-4	710	168	3.0	X	X				90	92-6	710	168	2.9	X	X				90
110-4	710	410	3.0		X	X			60	120-6	710	168	2.7	X	X				80
123-4	710	740	3.4		X	X		X	0	110-6	710	410	2.8			x		X	10
111-4	710	4320	3.0		X	X	x	X	0	123-6	710	740	3.0			X	X	X	1
102-4	665	722	4.7		X	X	X	X	0	111-6	710	4320	3.1			X	X	X	0
107-4	650	24	3.6						99	102-6	665	722	3.2			X	X	X	0
99-4	650	72	4.1		X				95	107-6	650	24	2.4	X					99
119-4	650	72	3.3		X				95	119-6	650	72	3.4	X	X				95
106-4	650	170	4.1		X				90	106-6	650	170	3.1	X	X				80
122-4	650	336	3.2		X				80	122-6	650	336	3.2				X	X	0
118-4	650	720	3.0				X	X	0	118-6	650	720	3.6				x	X	0
126-4	650	2206	3.2				X	X	0	126-6	650	2206	3.1				X	X	0
109-4	650	4314	3.3				X	X	0	109-6	650	4314	2.5					X	0
105-4	625	1656	4.5				X	X	0	105-6	625	1656	3.3				X	X	0
103-4	610	24	4.2						99	103-6	610	24	3.6	X					99
112-2	610	26	2.7						99	91-6	610	72	3.5		X				95
91-4	610	72	4.2		X				99	93-6	610	72	2.5		X				98
93-4	610	72	2.8		X				99	94-6	610	94	3.7	X	X				95
94-4	610	94	3.9		X				99	97-6	610	168	3.4	X	X			x	90
97-4	610	168	4.5		X				95	114-6	610	312	3.2		X			x	60
115-1	610	168	2.9		X				95	100-6	610	721	4.2				X	X	0
113-1	610	292	2.7		X				95	108-6	610	4320	2.3				X	X	0
114-4	610	312	3.1		X		X		95	116-6	597	720	3.5				X	X	0
100-4	610	721	4.5				X	X	0										
108-4	610	4320	2.8				X	X	0										
116-4	597	720	3.2				X	X	0										
Granite GR-2										**Granite GR-10**									
89-4	850	3	30.0	x					100	89-6	850	3	26.6	X					99
88-1	850	3	1.6						100	88-6	850	3	3.6	X					99
86-1	850	24	2.5	x					99	87-4	850	24	2.2	X	x				98
124-2	850	170	2.9	X					98	124-8	850	170	3.2	X	X				95
127-2	800	168	2.6	X					95	127-8	800	168	2.6		X				90
125-2	750	842	2.8	X	X				70	125-8	750	842	3.9		x			X	80
101-2	725	720	2.6	X	X		x	X	1	101-7	725	720	4.2		X			X	0
104-2	725	2157	2.8	X	X		x	X	1	104-8	725	2157	3.6		X			X	0
90-2	710	24	3.3	X					98	90-8	710	24	3.7	X					90
95-2	710	24	3.1	X	X				95	128-5	710	73	3.0	X	X				70
121-2	710	73	3.2		X			X	95	92-8	710	168	3.4		X			X	30
120-2	710	168	3.1	X		x			90	120-8	710	168	3.0	X	X			X	40
92-2	710	168	2.6	X					80	130-2	710	336	2.9		x			X	20
110-2	710	410	2.2				X	X	0	110-8	710	410	3.1					X	0
123-2	710	740	2.6				X	X	0	123-8	710	740	3.1					X	0
111-2	710	4320	2.4			X	x	X	0	111-8	710	4320	2.8					X	0
102-2	665	722	3.5				X	X	0	102-8	665	722	3.3			x	X	X	0
107-2	650	24	2.7	X	X				98	107-8	650	24	3.5						99
129-2	650	45	2.9	X					99	99-6	650	72	4.2	X	X				70
119-2	650	72	2.8		X			X	90	119-8	650	72	3.3	X	X				60
99-2	650	72	2.9		X			X	95	106-8	650	170	4.0			x	X	X	5
106-2	650	170	2.6	X	X			X	50	122-8	650	336	3.1				X	X	0
122-2	650	336	3.0				X	X	0	118-8	650	720	3.0				X	X	0
118-2	650	720	3.2				X	X	0	126-8	650	2206	2.9				X	X	0
126-2	650	2206	2.7				X	X	0	109-8	650	4314	2.8				x	X	0
109-2	650	4314	2.5				X	X	0	105-8	625	1656	3.2				X	X	0
105-2	625	1656	2.9				X	X	0	103-7	610	24	3.9						99
103-2	610	24	2.3	X					99	112-4	610	26	2.2		X				95
91-2	610	72	3.1	X	X				95	91-8	610	72	2.8		X				90
93-2	610	72	1.9	X	X				99	117-5	610	73	2.8		X				80
132-1	610	74	2.8	x					99	115-4	610	168	3.1		X		x	X	0
94-2	610	94	2.6		X				95	114-8	610	312	3.0				X	X	0

APPENDIX TABLE 1—*Continued*

Run no.	T (°C)	t (h)	H_2O (wt%)	Morphology HD	SK	GR	MP	AN	Approx. % glass
97-2	610	168	2.9		X				80
114-2	610	312	2.9		X				90
100-2	610	721	3.7				X	X	0
108-2	610	4320	2.1				X	X	0
116-2	597	720	3.0				X	X	0
Granite GR-1									
89-7	850	3	30.5	*x*					100
89-3	850	3	2.5	*x*					100
87-1	850	24	1.9	X					95
124-1	850	170	2.7	X					90
127-1	800	168	3.0	X					75
125-1	750	842	3.0	X	X				75
101-1	725	720	3.1			X		X	15
104-1	725	2157	2.9			X		X	5
95-1	710	24	3.1		X				90
90-1	710	24	3.1	X	X				90
98-1	710	72	2.4	X	X	*x*			80
121-1	710	73	2.8		X				70
120-1	710	168	3.1	X	X	X		X	50
92-1	710	168	2.4					X	30
110-1	710	410	2.1					X	0
123-1	710	740	3.1			X		X	0
111-1	710	4320	2.5			X		X	0
102-1	665	722	3.9		X	X		X	0
107-1	650	24	2.0	X					95
99-1	650	72	3.1		X				90
119-1	650	72	2.9		X				80
106-1	650	170	2.3			X		X	20
122-1	650	336	2.7					X	0
118-1	650	720	2.8			X		X	0
126-1	650	2206	2.8			X		X	0
109-1	650	4314	2.3					X	0
105-1	625	1656	3.8				X	X	0
103-1	610	24	1.7	X					95
112-1	610	26	2.7	X					95
91-1	610	72	3.2	X	X				90
117-1	610	73	2.5		X				90
94-1	610	94	1.6		X				95
97-1	610	168	2.9		X				70
114-1	610	312	2.4		X		X	X	10
100-1	610	721	3.7				X	X	0
108-1	610	4320	1.9					X	0
116-1	597	720	2.8				X	X	0
Granite GR-3									
89-2	850	3	3.2	X					80
87-2	850	24	3.7	X					70
124-3	850	170	3.1	X				X	60
127-3	800	168	3.0					X	50
125-3	750	842	3.0	*x*	X			X	40
104-3	725	2157	3.9					X	0
90-3	710	24	5.5		X			X	70
95-3	710	24	3.7		X			X	70
128-1	710	73	3.2		X			X	30
92-3	710	168	5.5		X			X	10
120-3	710	168	3.2		X			X	0
110-3	710	410	3.7		X			X	0
123-3	710	740	3.3		X			X	0
111-3	710	4320	2.9		X			X	0
102-3	665	720	4.3		X			X	0
107-3	650	24	3.0		X			X	40
99-3	650	72	5.0					X	0
119-3	650	72	3.2					X	0
106-3	650	170	4.2					X	0
122-3	650	336	3.1					X	0
118-3	650	720	3.2					X	0
126-3	650	2206	2.8					X	0
109-3	650	4314	2.8					X	0
105-3	625	1656	3.9					X	0
103-3	610	24	3.6		X			X	70
91-3	610	72	5.9		X			X	20
100-8	610	721	4.2				X	X	0
108-8	610	4320	2.3				*x*	X	0
116-8	597	720	3.0				X	X	0
Granite GR-7									
88-3	850	3	3.8	*x*					100
86-3	850	24	4.0	*x*					100
124-5	850	170	3.2	X					98
127-5	800	168	3.1	X					90
125-5	750	842	3.2	X				X	80
101-4	725	720	4.4	X		*x*		X	20
104-5	725	2157	3.8			X		X	10
90-5	710	24	4.4	X	X				95
95-5	710	24	4.2	X	X				95
98-5	710	72	7.0	X					90
128-2	710	73	3.0	X	X				60
121-5	710	73	3.2	X	X	*x*			70
92-5	710	168	3.9	X	X	*x*		X	60
120-5	710	168	3.2	X	X	*x*		X	70
110-5	710	410	3.5			X		X	5
123-5	710	740	3.2			X		X	1
111-5	710	4320	3.2			X		X	0
102-5	665	722	4.0			X	X	X	0
107-5	650	24	2.6	X	X				95
119-5	650	72	3.2	X	X				80
106-5	650	170	4.1	X	X	*x*		X	30
122-5	650	336	3.0				X	X	0
118-5	650	720	3.1				X	X	0
126-5	650	2206	3.2				X	X	0
109-5	650	4314	2.6					X	0
105-5	625	1656	4.2				X	X	0
112-3	610	26	2.6						100
91-5	610	72	5.3	X	X				90
117-3	610	73	3.2	X	X				95
93-5	610	72	3.0	X	X				95
94-5	610	94	3.6		X				90
97-5	610	168	4.7		X				90
115-2	610	168	3.1					X	70
114-5	610	312	3.4				X	X	0
100-5	610	721	5.6				X	X	0
108-5	610	4320	3.0				X	X	0
116-5	597	720	3.1				X	X	0
Granite GR-9									
89-5	850	3	26.3						80
88-5	850	3	2.2						80
87-3	850	24	2.4						80
124-7	850	170	3.3	X	X			X	70
127-7	800	168	3.0	X	X			X	60
125-7	750	842	3.4	*x*	*x*			X	60
101-6	725	720	3.6					X	0
104-7	725	2157	3.9					X	0
90-7	710	24	5.1	X	X				80
95-7	710	24	3.1	X	X			X	80
128-4	710	73	3.2	X	X			X	40
121-7	710	73	3.2	X	X			X	40
82-7	710	168	3.4					X	0
120-7	710	168	3.2					X	20
110-7	710	410	2.6					X	0
123-7	710	740	3.2					X	0
111-7	710	4320	2.6					X	0
102-7	665	722	3.7					X	0
107-7	650	24	2.6						50
99-5	650	72	4.4		X			X	10
119-7	650	72	3.5					X	5
106-7	650	170	3.6					X	0
122-7	650	336	3.1					X	0
118-7	650	720	3.0					X	0
126-7	650	2206	2.6					X	0
109-7	650	4314	2.4					X	0

APPENDIX TABLE 1—*Continued*

Run no.	T (°C)	t (h)	H_2O (wt%)	Morphology					Approx. % glass	Run no.	T (°C)	t (h)	H_2O (wt%)	Morphology					Approx. % glass
				HD	SK	GR	MP	AN						HD	SK	GR	MP	AN	
117-2	610	73	3.3		X			X	5	105-7	625	1656	4.2				X	X	0
132-2	610	74	3.1					X	5	103-6	610	24	3.4		X				70
94-3	610	94	3.5		X			X	0	91-7	610	72	4.3		X				70
97-3	610	168	3.3		*x*			X	0	117-4	610	73	3.2					X	0
114-3	610	312	3.5					X	0	115-3	610	168	2.9					X	0
100-3	610	720	4.5					X	0	114-7	610	312	2.9					X	0
108-3	610	4320	3.1					X	0	100-7	610	721	4.2					X	0
116-3	597	720	3.1					X	0	108-7	610	4320	2.3					X	0
										116-7	597	720	3.0					X	0

Note: HD = hexagonal dipyramids; SK = skeletal quartz; GR = granophyric quartz–feldspar intergrowths; MP = micropoikilitic quartz; AN = anhedral quartz; X denotes major morphologies; *x* denotes minor or rare morphologies and in experiments of short duration indicates that the phase could not be detected on an X-ray diffraction scan.